Available online at www.sciencedirect.com
SCIENCE DIRECT®
PERGAMON
Radiation Physics and Chemistry 68 (2003) 41–50
Radiation Physics and Chemistry
www.elsevier.com/locate/radphyschem

Dynamics of ionization processes studied with the COLTRIMS method—new insight into e–e correlation

H. Schmidt-Böcking[a,*], V. Mergel[a], L. Schmidt[a], R. Dörner[a], O. Jagutzki[b], K. Ullmann[b], T. Weber[a], H.J. Lüdde[c], E. Weigold[a,d], A.S. Kheifets[d]

[a] *Institut für Kernphysik, University of Frankfurt, August-Euler-Str. 6, 60486 Frankfurt, FRG, Germany*
[b] *Roentdek GmbH, 65779 Kelkheim, FRG, Germany*
[c] *Institut für Theor. Physik, Univ. Frankfurt, Robert-Mayer-Str. 8-10, 60487 Frankfurt, FRG, Germany*
[d] *Research School of Physical Science and Engineering, Australian National University, Canberra 0200, Australia*

Abstract

Many particle dynamics in atomic and molecular physics has been investigated by using the COLTRIMS method. The method and its power is discussed. The COLTRIMS technique visualizes many-particle fragmentation processes in the eV and sub milli-eV regime and reveals like the bubble chamber the complete momentum pattern in atomic and molecular particles reactions. Complete differential cross sections in momentum space have been measured for the transfer ionization channel in fast four-body ($p+He \rightarrow H^{\circ}+He^{2+}+e$) collisions. The correlated kinematical transfer ionization channel has been used to probe the highly correlated contributions to the asymptotic parts (high momenta and large nuclear impact parameters) of the He ground-state momentum wave function. In this reaction, one electron with selected initial momentum (2.5–7.5 a.u.) in the He ground state is kinematically captured by the proton (tunneling through the two-center barrier). The measured three-particle final-state momentum distributions show well-structured patterns, which reflect special features of the three-particle initial-state momentum wave function.

1. Introduction

Correlated many-particle dynamics in Coulombic systems, which is one of the unsolved fundamental problems in physics, can now be experimentally approached with so far unprecedented completeness and precision. The recent development of the COLTRIMS technique (COLd Target Recoil Ion Momentum Spectroscopy) (Ullrich et al., 1997; Dörner et al., 2000) provides a coincident multi-fragment imaging technique for eV and sub-eV fragment detection. In its completeness it is as powerful as the bubble chamber in high-energy physics. Based on state-of-the-art cooling techniques (super sonic jets, MOT etc.) and nuclear physics imaging methods, fragmentation processes of atoms, molecules, clusters, as well as of solid state surfaces induced by single photon or multi-photon laser absorption, electron or ion impact can be explored completely in momentum space and, for ions, with micro-eV resolution. In numerous benchmark experiments (Ullrich et al., 1997; Dörner et al., 2000), quasi-snapshots (duration as short as an atto-sec) of the correlated dynamics between electrons and nuclei had been made for atomic and molecular objects. This new imaging technique has opened a powerful observation window into the hidden world of many-particle dynamics. With the COLTRIMS reaction microscope, one can project the total global wave function, but also tiny fractions (here less than one part in 10^8) of the total momentum wave function onto a special kinematical final state.

Since the early days of atomic physics, the correlated momentum wave function of the He ground state remained as one of the unsolved fundamental puzzles in modern physics (Tanner et al., 2000). Correlation is particularly important, when the electrons are fast and

*Corresponding author.

0969-806X/03/$ - see front matter
doi:10.1016/S0969-806X(03)00254-8

when the asymptotic part of the wave function is considered. In investigating the ground-state binding energy by high-resolution spectroscopy one probes, however, the wave function at the region of the maximum density near the Bohr radius. The theoretical binding energies are obtained on the basis of a many-body approximation, such as the multi-configuration approach (MCA) (Kinoshita, 1959). Using variational methods a wave function is generated which requires a huge basis of diagonal and off-diagonal matrix elements, or as in nuclear physics on-shell and off-shell states. These off-diagonal matrix elements represent highly correlated virtually excited contributions to the He ground state, which cannot be described by He-independent-particle shell-model states. E.g., the lowest virtually excited p contributions for this He ground state are not the He 2p states but are pseudo-states (Stelbovics 1992; Fon et al., 1981; Scholz et al., 1991) in the field of a nucleus with a nuclear charge larger than the one of He. Since the He ground state is a $^1S_0$ state, the three-particle ground state can contain only strongly correlated s^2, p^2, etc. $^1S_0$ contributions and the MCA wave function can be separated into such angular momentum contributions. In MCA ground-state energy calculations the s^2 states contribute about 99% of the energy, the virtually excited p^2 about 1%, etc.

In correlated transfer ionization reaction channel (cKTI), the fast proton captures, by tunneling through the two-center Coulomb barrier, one He electron (named number 1) nearly exclusively into its ground state, while the remaining He^+ ion is left in a virtually exited state from which it instantaneously fragments due to a shake-off process leaving electron 2 in a continuum state. Thus, electron 2 is transferred from a *virtually* exited state to the real energy continuum in the final state with only a minor change of its momentum. Since the initial-state momentum of electron 1 can be determined from the final-state H° deflection angle (as shown below), the initial-state momentum correlation between electrons 1 and 2 can be directly revealed from the final-state momentum distributions obtained for the cKTI reaction channel (Mergel et al., 2001).

The electron transfer to the projectile can proceed via different reaction channels: (a) electron–electron–Thomas TI (eeTTI) (Mergel et al., 1997; Palinkas et al., 1989; Briggs and Taulbjerg, 1979; Ishihara and McGuire, 1988; McGuire et al., 1989, 1995; Shakeshaft and Spruch, 1979); (b) nucleus–electron–Thomas TI (nTTI) (Thomas, 1927, Horsdal-Pedersen et al., 1983; Vogt et al., 1986); and (c) kinematical capture (KTI) (Brinkman–Cramer type). While eeTTI always leads to a transfer ionization where the second electron is ejected, the KTI and nTTI processes are accompanied by ionization of the second electron either by shake-off via e–e correlation or by an independent binary collision of the proton with the second electron. All TI processes such as eeTTI and KTI followed by double scattering with the He nucleus will lead to characteristic locations in the final-state momentum phase space. The maxima of the distributions of the longitudinal H° final-state momentum and in particular of the recoil momentum provide a unique signature for the different TI channels, as will be detailed below. In order to distinguish the different channels experimentally, the projectile momentum transfer (the transverse and longitudinal component) has to be measured with extremely high resolution (about $0.3\,\text{a.u.} \approx 10^{-5}$ of the projectile momentum), which can never be achieved with standard techniques, but can easily be achieved by the COLTRIMS technique, where in inverse kinematics the recoil momentum is detected. The separation of the recoil energy between the channels is only of the order of a few meV.

2. Experimental technique

Using the high momentum resolution and high multi-coincidence efficiency of COLTRIMS, the complete final-state momentum distributions for fast (150–1400 keV) $p + He \rightarrow H^\circ + He^{2+} + e$ transfer ionization processes (TI) have been systematically measured by Mergel (Mergel et al., 1995) at the 2.5-MeV van-de-Graaf accelerator of the Institut für Kernphysik of the Universität Frankfurt. Details are given in Mergel (1996). The projectile beam was collimated to a diameter of <0.5 mm and a divergence of <0.25 mrad. The beam was charge state selected in front and behind the target region by different sets of electrostatic deflector plates. A supersonic helium gas jet is used as target, it combines the two most important features necessary for high-resolution recoil-ion spectroscopy: low internal temperature and localization of the target (diameter 5 mm). The helium gas is cooled down to 20 K before it expands through a 30 μm nozzle into the source chamber. During the expansion the gas cools down to an internal temperature of <50 mK. The gas jet is formed by passing through a 0.7 mm skimmer, located 6 mm from the nozzle, resulting in a jet diameter of 5 mm at the intersection with the ion beam. A residual gas pressure without gas jet of 1×10^{-8} mbar and a target density of $1.5 \times 10^{12}\,\text{cm}^{-2}$ were obtained. The recoil ions are extracted by a weak electric field (9 V/cm) transversely to the ion beam (see Chapter 2 of this book). The kinematics of the capture and TI reactions is described in detail in Mergel (1996).

In Fig. 1 the principle of the new reaction microscope (synonym: COLTRIMS) is presented. In a well-designed electric field configuration (static or pulsed), the positively as well as the negatively charged fragments are projected (typically with 4π solid angle) on two position-sensitive detectors. Measuring the impact

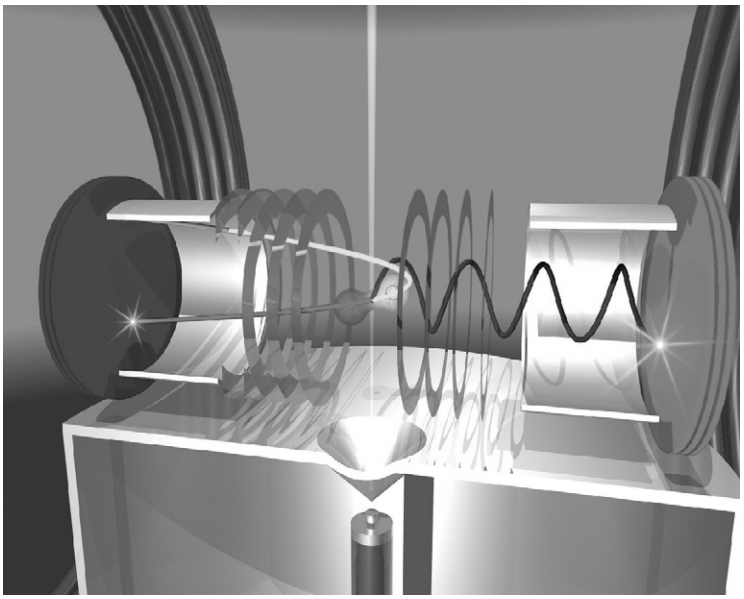

Fig. 1. Artist view of the COLTRIMS imaging system (Ullrich et al., 1997; Dörner et al., 2000).

position on the detector (typically $<0{,}1$ mm resolution) and the time-of-flight of the fragment (TOF) between the moment of fragmentation till hitting the detector, the particle trajectory, and thus the particle momentum after fragmentation, can be determined. To improve its momentum resolution electrostatic lenses can be incorporated into the projection system, such that the influence of the size of the target region, from where the fragments originate, can completely be eliminated (Mergel, 1996; Dörner et al., 2000; Ullrich et al., 1997).

To detect also the higher energetic electrons, magnetic fields, superimposed over the electric field (Ullrich et al., 1997), as well as pulsed electric fields can be used. If particle detectors based on fast delay-line position readout are used, multi-hit detection is possible. Even two particles hitting the detector at the "same" instant ($\Delta t<1$ ns) can simultaneously be detected. The number of detected multi-hits is practically only limited by the electronics needed to store in event mode all information. In future even up to 100 particles per micro-sec might be detectable if fast transient recorder units with channel resolution of about 0.1 ns become available. Thus, for low-energy particles (micro-eV to hundreds of eV) the COLTRIMS method is indeed as powerful as advanced bubble chamber systems for high energetic (MeV) particles. It is even comparable with modern time projection chamber systems used in high-energy physics. Furthermore, the rate of fragmentation processes per second can exceed several 100 kHz.

As a typical example for COLTRIMS data, Fig. 2 shows the recoil-ion momentum distribution of He^+ ions from the photoelectric effect at a single atom (the electric field vector of the linear polarized photon is parallel to the horizontal direction). This data set is simultaneously obtained for all momenta. Using COLTRIMS, the typical duration of such measurements is less than 1 h for data sets. The physics of these data is discussed in Dörner et al. (2000).

To demonstrate the wide application of COLTRIMS in Fig. 3 the angular distribution for K photoelectron emission for the reaction $\gamma+AB\rightarrow A^+ + B^+ + e_\gamma + e_{K-Auger}$ is shown (γ circular polarized). The molecular axis is oriented parallel to the electric field vector (z-axis). The circular polarization and the impact direction of the photon are indicated by the arrow. In this measurement, both photoelectron and recoil-ion momentum distribution are detected in coincidence and the digitized data are stored in list-mode technique.

3. Experimental results and discussion of observed momentum patterns

Our study of the TI process in p–He collisions was stimulated by the systematic work of Horsdal et al. (1986) and Giese and Horsdal (1988) on TI processes for p on He, who found a pronounced peak at about 6.5×10^{-4} rad in the H°-scattering-dependent ratio of TI to pure capture differential cross section. The peak maximum increased with projectile energy and reached about 25% at 1 MeV proton impact energy. Their observation contradicted all expectations, and was indeed very puzzling. Horsdal et al. explained their findings by a possible large contribution of eeTTI processes. Based on complete differential final-state momentum distributions Mergel et al. (2001) could

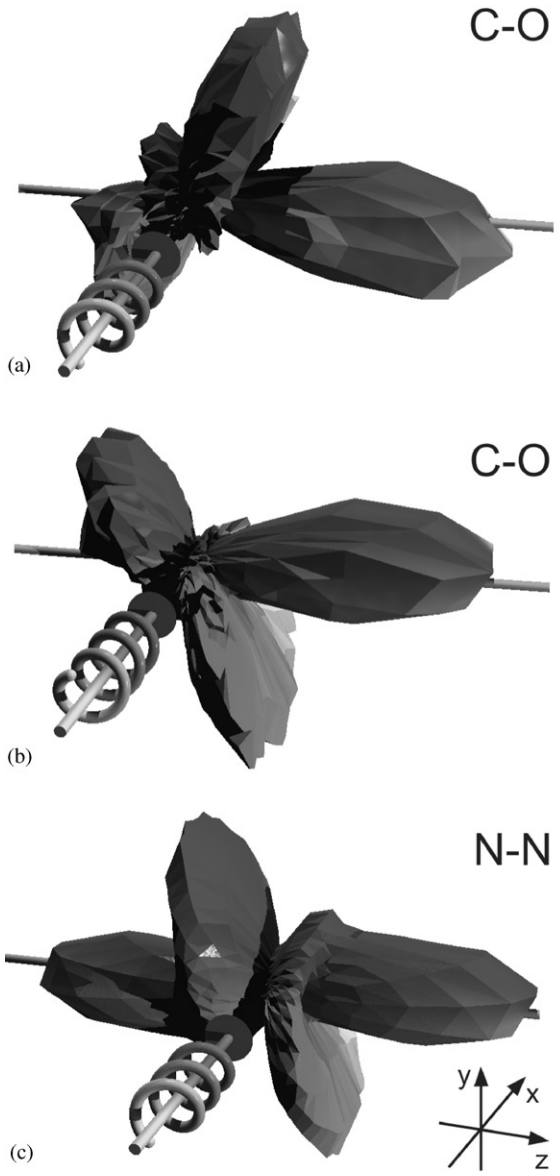

Fig. 2. Recoil-ion momentum distribution for single ionization of He induced by a single photon of 80 eV (Dörner et al., 2000).

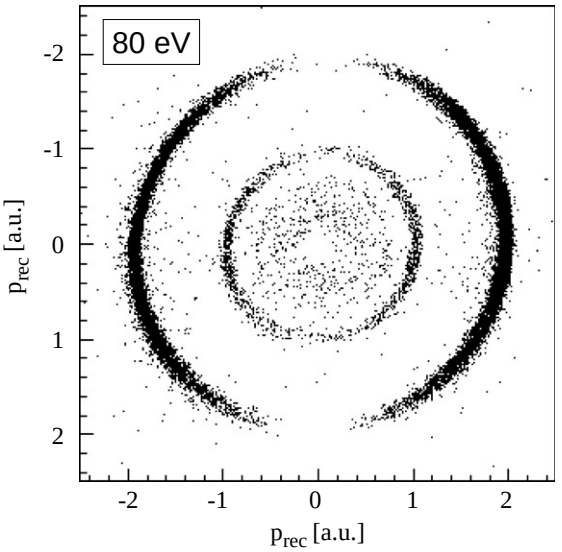

Fig. 3. Angular distribution for K photoelectron emission in diatomic molecules after K shell ionization by a circular polarized photon of 300 eV (Jahnke, 2002).

clearly show that neither eeTTI nor multiple scattering is responsible for the observed peak in the cross-section ratio, but could not present an explanation for this peak structure. As Mergel et al. (2001) have shown the main contributions to TI for the projectile velocities investigated here and thus also the puzzling structures observed by Horsdal et al. result from the cKTI process. The complete differential cross sections in momentum space of Mergel (2001, 1996) show some even more puzzling features of the momentum patterns namely:

(a) Electron 2 is predominantly emitted into the backward and negative k_x direction (see below for definition of the coordinate system), and the emission of electron 2 with respect to the outgoing H° is never into positive k_x direction, i.e. completely asymmetric.
(b) The He^{2+} momentum distribution and therefore also the electron 2 momentum distribution peak in the H° scattering plane.
(c) The ratio of cKTI to pure capture total cross sections increases with decreasing perturbation (increasing proton impact energy).
(d) Electron 1, recoil He^{2+}, and electron 2 always share comparable momenta. In particular, none of these particles in the final-state shows a momentum distribution peaking at zero. According to theoretical predictions (Kheifets, 2002; Shi and Lin, 2002), the momentum of shake electron 2 should peak near zero and the recoil k_r momentum would be expected to peak near $k_r = (0, 0, -v/2)$.

As shown in Mergel et al. (2001), these four observations cannot be explained by non-correlated particle dynamics of a proton interacting with a He nucleus and two uncorrelated s electrons. In particular, observation (b) (the four-particle planar final-state motion) requires a strong four-particle correlation in angular momentum. This angular momentum must already be present in the initial He ground state, since the momentum transfer of the proton to the He is small and thus also the angular momentum transfer is small ($\ll 1$ a.u.). This conclusion is supported by the

observation that at high E_p electron 1 is nearly exclusively captured into the projectile 1s state and in the pure capture channel electron 2 is very rarely excited into any higher $He^+(nl)$ state.

We will show below that the cKTI process for the proton impact energies investigated here proceeds nearly exclusively via shake-off processes from correlated non-s^2 contributions to the He ground state. Thus, fragmentation of the He^{1+} ion always occurs due to the angular momentum entanglement of the three He particles and not by interaction of the proton with electron 2. From the final-state momentum pattern of H°, He^{2+} and electron 2 we can deduce and directly reveal the part of the initial momentum wave function, which is dominated by non-s^2 contributions.

In Fig. 4 we show the single differential TI (right column) together with the corresponding pure capture (left column) cross sections as a function of the H° transverse momentum k_{x,H° (i.e. the scattering angle θ_P) for different proton impact energies (150–1400 keV). These data again agree within the experimental uncertainty with the results presented by Horsdal et al. (1986).

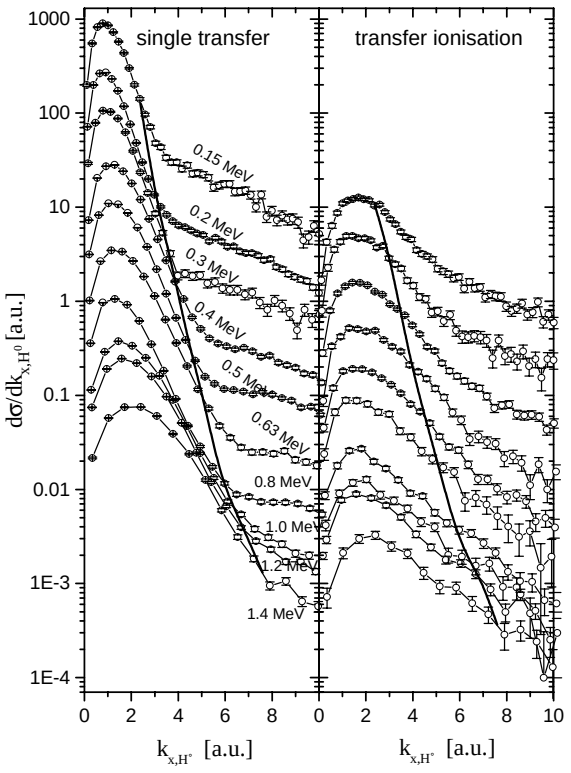

Fig. 4. Single differential TI (right column) together with the corresponding pure capture (left column) cross sections as a function of the H° transverse momentum k_{x,H° (i.e. the scattering angle θ_P) for different proton impact energies (150–1400 keV). The solid line indicates the maximal transverse momentum of a proton scattered on a free electron at rest.

Considering the H°-scattering-angle-dependent differential cross section for capture and TI (see Fig. 4) we see that both results show a large peak at very small scattering angles (below 0.6 mrad) and a smooth decrease of the cross sections above 1 mrad. This small angle peak accounts for nearly all protons scattered by electrons of the He atom. This explanation has been proven by calculations in which the nuclear–nuclear repulsion has been neglected (Gayet, 1989; Gayet and Salin, 1991a, b). As a result the small scattering angle part of the capture cross section remains almost unchanged in the relative H° scattering angle dependence and the shape of each peak reflects the electron transverse velocity distribution for the given projectile velocity v_p.

In the very small angle regime (the region of the peak) for most collisions the transverse nuclear momentum exchange is below 0.2 a.u. For Coulomb scattering at impact energies below 1 MeV this corresponds to impact parameters larger than the He K-shell radius. From the nuclear transverse momentum exchange (relation between recoil and projectile), we thus obtain information on the nuclear impact parameter range and indirectly also on the distance (close or distant) from the He nucleus where electron 1 is captured.

For the discussion of the fully differential final-state momentum pattern of the cKTI, a coordinate system is defined where the z-axis is the incoming projectile momentum $k_0 = m_p v_p$ and the H° projectile is always scattered into the positive x-direction. This coordinate system is obtained by rotating the laboratory system around the z-axis so that the y-component of the projectile momentum $k_{y,H}$ is always set to zero for each measured coincidence event.

In the capture channel below 6×10^{-4} rad the H° transverse momentum is nearly exclusively determined by momentum transferred by the captured electron. When electron 1 approaches the proton with $k_{x,e1}$, the deflected H° must conserve this component, thus being deflected by $k_{x,H} = k_{x,e1}$. Since for kinematical capture the longitudinal momentum component of the initial-state electron velocity should match the projectile velocity (overlap with the 1s state Compton profile of H°), the initial-state momentum vector k_{e1} of electron 1 can be approximately determined from the measured data by

$$\vec{k}_{e1} = \begin{pmatrix} k_{x,e1} \\ k_{y,e1} \\ k_{z,e1} \end{pmatrix} = \begin{pmatrix} k_{x,H} \\ 0 \\ v_p \end{pmatrix}. \quad (1)$$

For the pure capture channel, the maximum transverse momentum of H° due to scattering on the electron is therefore $k_{x,H} \approx m_e v_p$ in nearly perfect agreement with the data. For the cKTI process the proton is scattered from a correlated "electron pair" (*a quasi-heavy boson*),

thus the peak regime of θ_P can extend to about 1 millirad, which is twice the angle of the maximum deflection by a single electron.

The solid lines in Figs. 5 and 6 define the k_x and k_z zero positions. The recoil momentum in beam direction $k_{z,\mathrm{rec}}$ can be expected to be close to that for pure single capture. This momentum which is given by energy and momentum conservation is

$$k_{z,\mathrm{He+}} = -m_e v_p/2 - Q/v_p, \quad (2)$$

where $Q = -2.9$ a.u. (see Mergel (1996) and Dörner et al. (2000) for the kinematics). This $k_{z,\mathrm{He+}}$ value is indicated by the dashed lines in Fig. 5. In a TTI process, however, the momentum exchange is a sequence of close binary Coulomb collisions and the recoil yields a completely different momentum pattern in the final state compared to cKTI processes.

In Fig. 5 data for larger H° angles are shown, where transverse nuclear momentum exchange dominates. Only one recoil peak is seen and all recoil momenta are close to the location (+) predicted by CTMC calculations (Mergel et al., 1997) for uncorrelated nTTI and KTI processes. The recoil momentum location agrees well with the expected location, but it is slightly shifted by about 1 a.u. into forward direction k_z (longitudinal position). The areas between the dashed and dotted lines represent the window corresponding to the negative H° transverse momenta. Indeed three peaks are seen, peak 1 represents the KTI- and nTTI-channel near the expected location (+), where again the H° transverse momentum results from nuclear scattering. Peak 2 represents the eeTTI (Mergel et al., 1997). Its measured kinematical location also agrees with the expected values. For eeTTI the recoil ion is mainly a spectator and the recoil momentum location is expected at small positive k_z and small negative k_x in agreement with our measurement. In Fig. 5c data for the small H° angular regime are shown, where the proton is mainly scattered by electron 1. Two peaks are seen, one at ($k_x = -1$ a.u., $k_z = +1$ a.u.) which is the eeTTI channel (Mergel et al., 1997). Peak 3 in Fig. 5c (like peak 3 in Fig. 5b) represents the cKTI channel. Their locations are contradictory to the predictions for any known uncorrelated TI process, which should be located between the dashed and dotted lines.

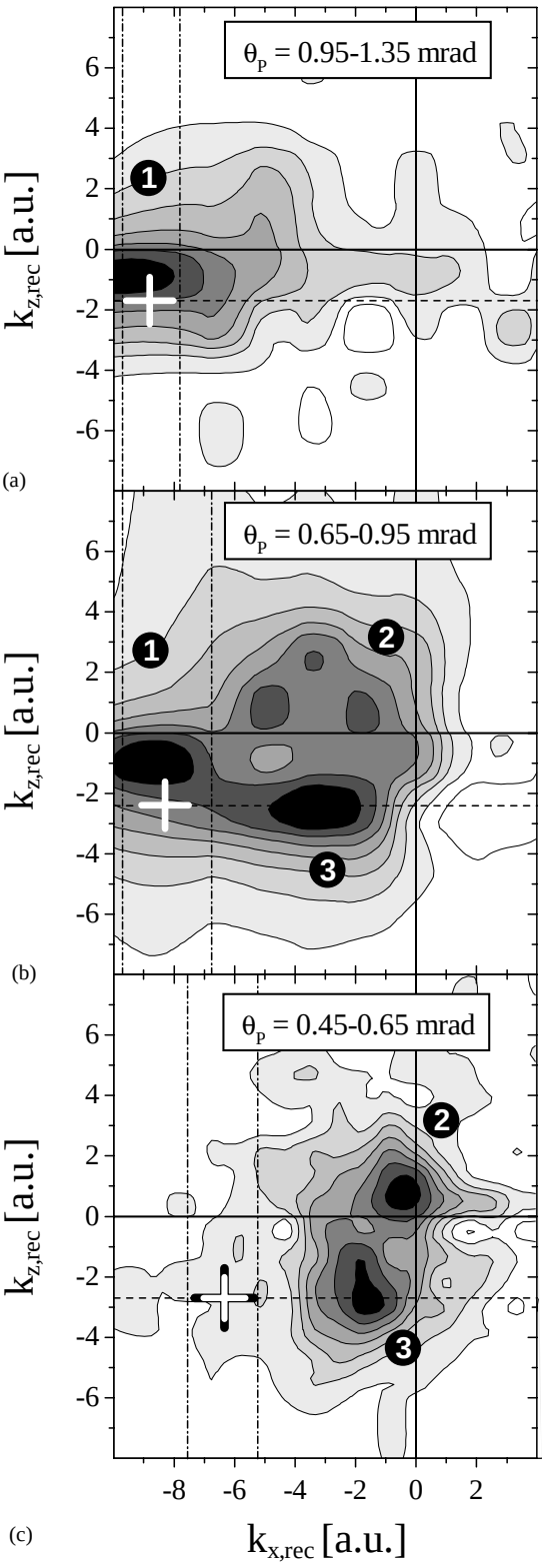

Fig. 5. Differential recoil ion TI cross sections projected on the H° scattering plane for selected projectile velocities and H° transverse momenta ((a) 0.5 MeV, (b) 0.8 MeV, and (c) 1 MeV). The solid lines represent $k_{z,\mathrm{rec}} = 0$, $k_{x,\mathrm{rec}} = 0$, the dashed lines the He^{1+} recoil momentum in the laboratory frame for the pure electron capture into the H° ground state, the areas between the dashed dotted lines the window for the negative H° transverse momenta, the "+" symbol the location calculated by CTMC method for the channels nTT and KTI. The locations of the observed peaks 1–3 are discussed in the text.

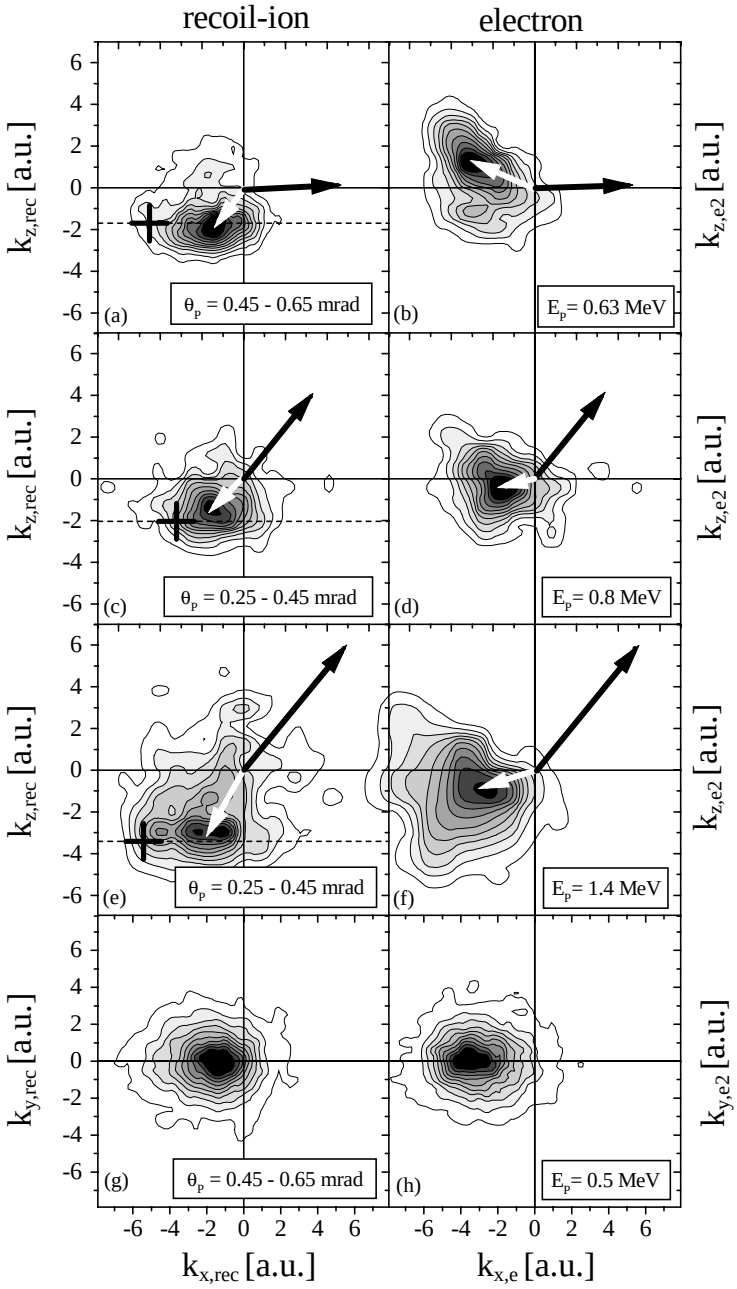

Fig. 6. Differential recoil ion (left column) and electron (right column) TI cross sections projected on the H° scattering plane for 630 keV impact energy at $\theta_P = 0.45-0.65$ mrad (a and b), in c and d for 800 keV $\theta_P = 0.25-0.45$ mrad, and in e and f for 1400 keV $\theta_P = 0.25-0.45$ mrad. The solid lines represent $k_z = k_x = 0$ and the dashed lines the He^+ recoil momentum in the laboratory frame for the pure electron capture into the H° ground state. The black vectors indicate the mean electron 1 momentum vector in the initial state, the white vectors represent the mean measured recoil momenta, the "+" symbol the expected location of nTTI and nKTI channels. In figure g and h the differential recoil and electron cross sections perpendicular to the beam direction are shown.

In Fig. 6 the corresponding triple differential recoil ion (left column) and electron (right column) cross sections projected on the H° scattering plane are presented. (In Figs. 6a and b for 630 keV impact energy at $\theta_P = 0.45-0.65$ mrad, in Figs. 6c and d for 800 keV at $\theta_P = 0.25 - 0.45$ mrad, and in Figs. 6e and f recoil and electron 2 momenta for 1400 keV at $\theta_P = 0.25 - 0.45$ mrad.)

Since for both the recoil ion and electron 2 one observes momentum distributions which are not rotationally symmetric with respect to k_{e1} momentum exchange of the proton with the α nucleus and electron 2 must be correlated.

It is obvious from Fig. 6 that the recoil and electron momenta have well localized positions in the H° scattering plane. Furthermore, both vector distributions peak exactly the H° scattering plane. This is evident from Figs. 6g and h, where the corresponding azimuthal angular distributions of recoil and electron (2) momenta for a typical case of $E_p = 500$ keV are plotted.

4. Shake-off process from non-s^2 contributions

Before we discuss the measured fully differential momentum distributions, the shake-off ratios (ratio between TI and single capture differential cross sections as a function of the H° scattering angle) in Fig. 7 will be compared with theory (Kheifets, 2002). As in the standard shake-off theory (Shi and Lin, 2002), we estimate the probability of the cKTI process as a double overlap integral:

$$\langle k_1 k_2|\Phi_0\rangle = \sum_{nl} A_{nl} C^{00}_{lm,l-m} \langle k_1|nlm\rangle \langle k_2|nl-m\rangle. \quad (3)$$

Here we make a multi-configuration Hartree–Fock expansion of the He atom ground state. Configuration interaction coefficients are falling off rapidly with increasing n,l, the leading terms being $A_{1s} = 0.996$, $A_{2s} = -0.059$, $A_{2p} = 0.059$, $A_{3d} = -0.012$. The Clebsch–Gordan coefficient couples the two individual electron angular momenta to the zero angular momentum of the He atom. In the first overlap integral we assume that the electron is picked up by the proton at a finite distance from the He nucleus:

$$\langle k_1|nlm\rangle = C_{lm} \int_{a>0}^{\infty} \mathrm{d}x\, \mathrm{e}^{\mathrm{i}k_{1x}x} \int_{-\infty}^{\infty} \mathrm{d}z\, \mathrm{e}^{\mathrm{i}k_{1z}z} R_{nl}(r) \mathrm{e}^{\mathrm{i}m\phi}, \quad (4)$$

where a is the impact parameter. Here we also choose the angular momentum quantization axis in the y-direction and write the electron wave function in the scattering plane as $\psi_{nlm}(r) = R_{nl}(r) Y_{lm}(\theta = \pi/2, \phi) = C_{lm} R_{nl}(r) \exp(\mathrm{i}m\phi)$, $\tan\phi = x/z$. In the second overlap $\langle k_2|nl-m\rangle$ the integration is expanded over the whole scattering plane and the final state $\langle k_2|$ is treated as the Coulomb wave in the He^{2+} field.

In the standard shake-off theory the x integration in Eq. (4) is expanded over the whole scattering plane and the integral becomes symmetric with respect to the sign reversal of m. In the cKTI theory, there is a very large asymmetry between $\pm m$ components $|\langle k_1|nlm\rangle / \langle k_1|nl-m\rangle| \sim k_{1z}a \gg 1$. This asymmetry can be understood if one remembers that the departing electron carries away the classical angular momentum $k_{1z}a$ and the projection of this momentum on the quantization axis favors only one particular sign of m. The large angular momentum $k_{1z}a \gg 1$ has to be drawn from a ground state orbital with a limited l,m. This makes the overlap integral exponentially small $\langle k_1|nlm\rangle \sim \exp(-k_{1z}a)$. This smallness is offset by a growing power term $(\beta a)^l$ where β is the exponential fall-off parameter of the radial orbital $R_{nl}(r)$ (see Kheifets (2002) for more details). The power term compensates the small coefficients A_{nl} for $l > 0$. As a result, the strongest contribution to the amplitude Eq. (4) comes from the $2p_{+1}$ and $3d_{+2}$ terms but not the 1s one.

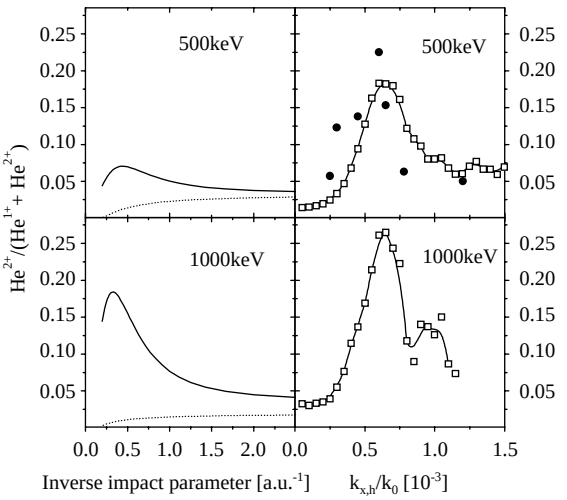

Fig. 7. Ratio of H° scattering angle ($\theta_P = k_{x,H}/k_0$) TI differential cross sections (this work, open squares; Giese and Horsdal, solid circles) to the sum of pure capture plus TI cross sections for different projectile energies (right column: experiment, left column: theory).

In Fig. 7 (right column) the experimental ratios for 500 and 1000 keV proton impact energy are shown as a function of the measured H° scattering angles ($\theta_P = k_{x,H}/k_0$, unit millirad). In the left column the theoretical predictions are presented (dashed line: only s^2 contributions, solid line: including non-s^2 contributions) as a function of the inverse impact parameter, which for pure nuclear scattering is proportional to the transverse momentum. The abscissa of both figures can only be qualitatively compared, since in the experimental data above 1.3 millirad the H° deflection is due to Rutherford scattering of both nuclei, (thus this regime corresponds to small impact parameter (≈ 0.1 K shell radius)) and below 1 millirad the H° is scattered on the electrons only (thus the nuclear impact parameter should be large (> 1 a.u.)). The striking difference in the calculations for pure s^2 and non-s^2 contributions proves that the puzzling peak first observed by Giese and Horsdal (1988) can be related to capture and subsequent shake-off of paired non-s^2 electrons. The

theory even gives tentative agreement in the absolute height. This indicates that the cKTI process indeed probes the non-s^2 contributions of the ground-state He momentum wave function.

It is, however, not possible to reveal the details of the correlated non-s^2 wave function from the measured fully differential cross sections in comparison with theory. We find that the present calculations (Kheifets, 2002; Shi and Lin, 2002) can only partially describe the observed momentum pattern.

Based on a proton straightline trajectory the calculations predict four characteristic features:

(a) only $m = +1$ contributions can be captured into the fast moving proton, thus, electron 2 is very asymmetrically emitted (only opposite to the deflected proton towards negative k_x);
(b) momenta of recoil and electron 2 are coplanar in the H° scattering plane;
(c) at large impact parameters for the impact energies investigated here the non-s^2 contributions to the cKTI process dominate; and
(d) for both s^2 and non-s^2 components the emitted electron 2 momentum peaks near zero.

Prediction a–c are in agreement with the data:

(a) the measured final-state momentum distributions in the nuclear H° scattering plane (the nuclear angular momentum vector) are strongly asymmetric below 0.6 mrad, i.e. they show an orientation with respect to the deflected H°;
(b) electron 2 and recoil are coplanar in the H° scattering plane;
(c) the cKTI contribution yields more than 85% of the total TI cross section; but
(d) the data are in clear contradiction to the theory-predicted low shake-off energy (prediction d).

Experimentally we find that cKTI never yields electron momenta peaking near zero. As seen in Figs. 5 and 6 the energy of electron 2 even increases with increasing impact energy and with increasing H° angle (below 0.6 mrad). The present theory cannot explain, why the shake-off electron 2 kinetic energy is never close to zero and exceeds 200 eV in many cases.

We note that the non-s^2 angular momentum is not transferred from the proton to any electron, but is provided by the initial He ground state. This conclusion is supported by experimental and theoretical investigations of the pure electron capture process of fast protons on He (Mergel et al., 1995; Gayet and Salin, 1991b). These authors show that the internal electronic excitation, i.e. the excitation of electron 2 into the He p state and the capture of electron 1 into any excited H° state, is negligibly small for the fast collision systems investigated here. Therefore, the required angular momentum transfer can only be provided from initial-state properties of the captured electron. If the electron is initially in an entangled p^2 or d^2 state the electron 1 can indeed provide the required angular momentum. Since the two electrons have to couple to an $^1S_0$ state, the angular momentum of electron 2 must be anti-parallel to that of electron 1 at all times. A cKTI process proceeding via p^2 electrons (with negligibly small momentum and angular momentum exchange between proton and He) could thus indeed explain the observation of a four-body (p + e1 + e2 + α-nucleus) coplanar fragmentation.

5. Conclusions

We conclude that the puzzling structures observed by Mergel et al. (2001) and Giese and Horsdal (1988) can be qualitatively explained by the cKTI process proceeding via selected shake-off processes from non-s^2 components in the asymptotic part of the He ground-state wave function. Several experimental observations can be qualitatively explained by the theory: (a) the puzzling peak in the angle-dependent ratio of TI to sum of TI + capture; (b) the observed asymmetry in electron 2 emission; and (c) the coplanar emission pattern of recoil electron 2 and scattered H°. However, the large electron 2 momenta are in clear contradiction to theory.

It is interesting to note that in classical mechanics such a scaling was predicted for the He ground state by Sommerfeld (1923). When the two He electrons move on two opposite (180°) elliptic orbits with the nucleus at rest, they can never fulfil simultaneously momentum and angular momentum conservation. They need a nucleus for compensation of momentum, which is then more easily fulfilled, if the axes of the electron ellipses are not intersecting by 180° but by a smaller angle between 90° and 150°.

Furthermore, we have shown that the non-s^2 contributions in the He ground-state wave function are not purely mathematical constructs in the virtually excited space, but have measurable consequences. These off-diagonal non-s^2 components seem to hide interesting properties with respect to the secret world of correlation. These states have classically seen a huge amount of kinetic energy, thus they are called highly virtually excited continuum states. These very fast electrons at large distance from the He nucleus are those with the strongest dynamical e–e correlations. Classically seen here the negative Coulombic energy is more than a factor 10 smaller than the positive kinetic energy of the fast electrons in a non-s^2 state. Generally physicists assume that the far distant part of the He ground-state wave function should contain slow moving electrons (otherwise the electrons could escape), but we deduce

from our data that the tiny fractions of the far distant wave function contain very fast, nearly relativistically moving electron pairs.

Both electrons occupy the non-s^2 state of motion together simultaneously with the nucleus, since the He ground state is a $^1S_0$ state. Generally, one would call such a two-electron system a pairing state (e.g. like a Cooper pair in a solid); however, this is misleading and overlooks the most important reason for that entanglement. It is the coupling of both electron momenta and angular momenta to the nuclear motion (nucleus is never at rest.). It is well known for superconductivity that phonon coupling to the solid (isotope effects) is very important. We see here for the He system that beside entanglement in momentum ($\Rightarrow$ phonon coupling), the angular momentum entanglement is even more important. Therefore, also for superconductivity and the quantized Hall effect (in particular the fractional Hall effect), angular momentum entanglement might be crucial for the existence of such dynamically entangled systems. Using COLTRIMS even such tiny fractions can be revealed.

Many new applications for COLTRIMS in different areas of AMOP physics are underway. Experiments of atomic and molecular fragmentation processes in strong femtosec laser pulses have recently been performed yielding precise information on sub-femtosec dynamics of the correlated motion of electrons and nuclei in strong laser pulses. The detection of fragmentation of BE condensates is in preparation. Last not least the fragmentation of biological species prepared in a gas jet or sitting on a surface are interesting applications for the COLTRIMS imaging method.

Acknowledgements

We acknowledge the numerous fruitful disputes and discussions with our colleagues and friends: V.M. acknowledges the support by the Studienstiftung des Deutschen Volkes and E.W. by the Humboldt-Stiftung. This work was supported by the DFG, the BMBF, GSI-Darmstadt, Graduiertenprogramm des Landes Hessen, DAAD and Roentdek GmbH.

References

Briggs, J.S., Taulbjerg, K., 1979. J. Phys. B 12, 2565.

Dörner, R., Mergel, V., Jagutzki, O., Spielberger, L., Ullrich, J., Moshammer, R., Schmidt-Böcking, H., 2000. Phys. Rep. 330, 96–192.

Fon, W.C., Berrington, K.A., Burke, P.G., Kingston, A.E., 1981. J. Phys. B 14, 1041.

Gayet, R., 1989. J. Phys. C 1, 53–70.

Gayet, R., Salin, A., 1991a. In: Bereny, D., Hock, G. (Eds.), High-Energy Ion–Atom-Collisions and Proceedings of the Fourth Workshop, Debrecen, September 1990, Lecture Notes in Physics, Vol. 376. Springer, Berlin, Heidelberg.

Gayet, R., Salin, A., 1991b. Nucl. Instrum. Methods B 56, 82–85.

Giese, J.P., Horsdal, E., 1988. Phys. Rev. Lett. 60, 2018.

Horsdal, E., Jensen, B., Nielsen, K.O., 1986. Phys. Rev. Lett. 57, 1414–1416.

Horsdal-Pedersen, E., Cocke, C.L., Stöckli, M., 1983. Phys. Rev. Lett. 50, 1910–1913.

Ishihara, T., McGuire, J.H., 1988. Phys. Rev. A 38, 3310–3318.

Jahnke, T., et al., 2002. Phys. Rev. Lett. 88, 073002.

Kheifets, A.S., 2002. Private communication, in preparation.

Kinoshita, T., 1959. Phys. Rev. 115, 366.

McGuire, J.H., Straton, J.C., Axmann, W.J., Ishihara, T., Horsdal, E., 1989. Phys. Rev. Lett. 62, 2933–2936.

McGuire, J.H., Berrah, N., Bartlett, R.J., et al., 1995. J. Phys. B 28, 913.

V. Mergel, 1996. Ph.D. Thesis, Universität Frankfurt, Shaker Verlag, ISBN 3-8265-2067-X.

Mergel, V., Dörner, R., Ullrich, J., Jagutzki, O., Lencinas, S., Nüttgens, S., Spielberger, L., Unverzagt, M., Cocke, C.L., Olson, R.E., Schulz, M., Buck, U., Zanger, E., Theisinger, W., Isser, M., Geis, S., Schmidt-Böcking, H., 1995. Phys. Rev. Lett. 74, 2200–9132203.

Mergel, V., Dörner, R., Achler, M., Khayyat, Kh., Lencinas, S., Euler, J., Jagutzki, O., Nüttgens, S., Unverzagt, M., Spielberger, L., Wu, W., Ali, R., Ullrich, J., Cederquist, H., Salin, A., Olson, R.E., Belkíc, Dvz., Cocke, C.L., Schmidt-Böcking, H., 1997. Phys. Rev. Lett. 79, 387.

Mergel, V., Dörner, R., Khayyat, Kh., Achler, M., Weber, T., Jagutzki, O., Lüdde, H.J., Cocke, C.L., Schmidt-Böcking, H., 2001. Phys. Rev. Lett. 86, 2257.

Palinkas, J., Schuch, R., Cederquist, H., Gustafsson, O., 1989. Phys. Rev. Lett. 63, 2464–2467.

Scholz, T.T., Walters, H.R.J., Burke, P.G., Scott, M.P., 1991. J. Phys. B 24, 2097.

Shakeshaft, R., Spruch, L., 1979. Rev. Mod. Phys. 51, 369–405.

Shi, T.Y., Lin, C.D., 2002. Phys. Rev. Lett. 89, 163202.

Sommerfeld, A., 1923. J. Opt. Soc. Am. 7, 509.

Stelbovics, A.T., 1992. In: MacGillivray, W.R., McCarthy, I.E., Standage, M.C. (Eds.), Invited Paper, Proceedings of the ICPEAC 1991. IOP Bristol, England, p 21, SSBN 0-7503-0167-8.

Tanner, G., Richter, K., Rost, J.M., 2000. Rev. Mod. Phys. 72, 497.

Thomas, L.H., 1927. Proc. Roy. Soc. A 114, 561–576.

Ullrich, J., Moshammer, R., Dörner, R., Jagutzki, O., Mergel, V., Schmidt-Böcking, H., Spielberger, L., 1997. J. Phys. B 30, 2917–2974.

Vogt, H., Schuch, R., Justiniano, E., Schulz, M., Schwab, W., 1986. Phys. Rev. Lett. 57, 2256–2259.